Controlling bulk Cu_6Sn_5 nucleation in Sn0.7Cu/Cu joints with Al micro-alloying

J.W. Xian[1,a], S.A. Belyakov[1] and C.M. Gourlay[1]

[1] Department of Materials, Imperial College

London, SW7 2AZ, UK

[a] jingwei.xian11@imperial.ac.uk

Abstract

We show that dilute Al additions can control the size of primary Cu_6Sn_5 rods in Sn-0.7Cu/Cu ball grid array (BGA) joints. In Sn-0.7Cu-0.05Al/Cu joints, the number of primary Cu_6Sn_5 per mm^2 is ~7 times higher and the mean three dimensional (3D) length of rods is ~4 times smaller than in Al-free Sn-0.7Cu/Cu joints, while the area fraction of primary Cu_6Sn_5 is similar. It is shown that epitaxial nucleation of primary Cu_6Sn_5 occurs on δ-$Cu_{33}Al_{17}$ or γ_1-Cu_9Al_4 particles, which are stable in the Sn-0.7Cu-0.05Al melt during holding at 250°C. The observed facet relationships agree well with previously determined orientation relationships between δ-$Cu_{33}Al_{17}$ and Cu_6Sn_5 in hypereutectic Sn-Cu-Al alloys and result in a good lattice match with <~2.5% lattice mismatch on two different interfacial planes.

1. Introduction

In the pursuit of next-generation Pb-free solders, there is ongoing interest in micro-alloying solders with Al [1-6]. Potential benefits of dilute Al additions include (i) the suppression of nucleation undercooling for βSn in Sn-Ag-Cu [1, 2] and Sn-Ag [3] solders, which has been linked to a reduction in primary (pro-eutectoid) Ag_3Sn blade formation [4] and may have the potential to grain refine the βSn phase in solder joints [5]; (ii) the suppression of Cu_6Sn_5 layer growth on Cu substrates [6]; and (iii) the introduction of small, hard Cu-Al intermetallics that could be harnessed as a dispersion in the βSn matrix to improve the performance and reliability of solder joints [5].

It has also been found that Al additions have a substantial influence on Cu_6Sn_5 in bulk solders [2, 4, 5, 7, 8]. Reeve et al. [5] and Boesenberg et al. [4] found that Cu_6Sn_5 often shared an interface with δ-$Cu_{33}Al_{17}$ in Sn-3.5Ag-0.95Cu, Kantarcıoğlu and Kalay [2] observed that 0.05 wt% Al additions reduce the size of Cu_6Sn_5 in Sn-3.5Ag-0.9Cu/Cu joints, and McDonald et al. [8] and Xian et al. [7] reported that Al micro-alloying decreased the size of primary Cu_6Sn_5 in hypereutectic Sn-4Cu alloys. The grain refinement and reduced nucleation undercooling of primary Cu_6Sn_5 due to Al additions has been deduced to be due to heterogeneous epitaxial nucleation of Cu_6Sn_5 on either δ-$Cu_{33}Al_{17}$ or γ_1-Cu_9Al_4 [7]. These two Al-Cu intermetallics have very similar crystal structure [7, 9, 10] and it was shown that both can form interfaces with only ~2.5% lattice mismatch to the first order and second order prism planes of Cu_6Sn_5 (i.e. the $\{1\bar{1}00\}$ and $\{11\bar{2}0\}$-type planes of Cu_6Sn_5) [7].

The crystallographic study on the nucleation of Cu_6Sn_5 on δ-$Cu_{33}Al_{17}$ or γ_1-Cu_9Al_4 particles was performed on large (0.5g) samples of Sn-4Cu-xAl and did not involve a solder substrate [7]. Common solders such as Sn-0.7Cu and Sn-3Ag-0.5Cu are

hypoeutectic (i.e. are in the βSn primary phase field of the liquidus projection) and primary Cu_6Sn_5 can only form if the nucleation undercooling for βSn is sufficiently high. In joints on Cu substrates, primary Cu_6Sn_5 formation is more complex because Cu-dissolution from the substrate produces a Cu_6Sn_5 reaction layer and also increases the Cu content in the liquid prior to solidification.

This paper builds on [7] to investigate whether dilute Al additions can be used to control the size of primary Cu_6Sn_5 in the more complex situation of Sn-0.7Cu/Cu ball grid array (BGA) solder joints. Since primary Cu_6Sn_5 formation is expected to depend on Cu dissolution from the substrate, the presence of a Cu_6Sn_5 layer and on Al additions, both (i) Sn-0.7Cu and Sn-0.7Cu-0.05Al freestanding BGA balls and (ii) Sn-0.7Cu/Cu and Sn-0.7Cu-0.05Al/Cu BGA joints are studied.

2. Methods

Sn-0.7Cu and Sn-0.7Cu-0.05Al (in mass%) solder balls were prepared by mixing 99.9 Sn ingots with Sn-10Cu and/or Sn-1Al master alloys in a graphite crucible and heating to 450°C in a resistance furnace. Molten samples were held for 60 minutes before being cast into a steel chill mould. The casts were then rolled down to foil ~30µm thick and punched into Ø1.6mm discs. Utilizing surface tension, ~500µm solder balls were then produced by melting the ~0.5mg discs with RM-5 flux on a hot plate at 350°C.

Using lithography, 0.5mm thick Cu substrates were covered with a solder mask patterned with circular holes 500µm wide. The solder balls were placed on the Cu substrates fluxed with RM-5 flux. Samples were then reflowed through a LFR400HTX TORNARDO reflow oven (Surface Mount Technology, Isle of Wight, UK). The thermal history was recorded by thermocouples attached to the carrier plate on the conveyor, showing that the samples were heated at ~2K/s up to a peak temperature of

248°C, spent ~58 seconds above the Sn-Cu_6Sn_5 eutectic temperature and were cooled at ~4.5K/s from 240-200°C. The joints were washed in ethanol to remove residual flux in an ultrasonic bath for 20 min.

Both freestanding solder balls and BGA joints were solidified in a Mettler Toledo DSC. The solder balls were placed in Al_2O_3 pans and cycled twice with a heating rate of 0.16K/s, a peak temperature of 250°C and a cooling rate of 0.33K/s. Solder joints underwent a final controlled reflow cycle in the DSC following the same thermal profile as the freestanding solder balls.

In order to test whether any solid phases were present at the peak reflow temperature, a holding experiment at 250°C using ~40g Sn-0.7Cu-0.05Al alloy was also performed. The alloy was cast into a cylindrical graphite mould which was then sealed in a quartz tube filled with Ar gas. The sample was then put in a forced air convection oven at 250°C for one week before being cooled at room temperature.

Samples were mounted in Struers VersoCit acrylic cold mounting resin and ground and polished following standard procedures. An Olympus DP70 optical microscope and a Zeiss Auriga field emission gun scanning electron microscope (FEG-SEM) were used to investigate the microstructure. The SEM is equipped with an Oxford Instruments INCA 80mm^2 x-sight energy dispersive X-ray (EDX) detector and a Bruker electron backscatter diffraction (EBSD) detector. Kikuchi patterns were analysed using Bruker Esprit software.

The three-dimensional morphology of Cu_6Sn_5 was investigated by selectively etching the Sn-0.7Cu and Sn-0.7Cu-0.05Al BGA balls and joints. A solution of 5% NaOH and 3.5% orthonitrophenol in distilled H_2O was used at 60°C for 15~30 min. Only the Sn

matrix was dissolved in the etchant and the single crystal intermetallics (both primary and eutectic) were later tipped onto a stub and studied in the FEG-SEM.

3. Results and Discussion

3.1. Sn-0.7Cu and Sn-0.7Cu-0.05Al BGA balls

Figure 1 shows optical micrographs of cross sections of Sn-0.7Cu and Sn-0.7Cu-0.05Al freestanding solder balls. Primary Cu_6Sn_5 crystals can be observed clearly in Sn-0.7Cu as labelled by the arrows in Figure 1 (A), but it is not obvious whether there are any primary Cu_6Sn_5 crystals in the cross section of Sn-0.7Cu-0.05Al in Figure 1 (B). Figure 1 (C) and (D) show typical Cu_6Sn_5 single crystals after the tin matrix was dissolved. The Cu_6Sn_5 crystals extracted from Sn-0.7Cu solder balls in Figure 1 (C) are long faceted rods and are clearly a primary (i.e. pro-eutectic) phase. The largest Cu_6Sn_5 in Sn-0.7Cu-0.05Al are much smaller and only weakly-faceted (Figure 1 (D)). Care was taken to check that no larger Cu_6Sn_5 crystals exist than the ones shown in Figure 1 (D).

To compare the extracted Cu_6Sn_5 with eutectic Cu_6Sn_5, a cross section of a Sn-0.7Cu-0.05Al freestanding ball was shallow etched for <1 min and is shown in Figure 2. From the higher magnification micrograph in Figure 2(B), it can be seen that the eutectic Cu_6Sn_5 has typical morphologies of both long needles and thin sheets, some of which are as long as ~60 μm. Additionally, in some regions the eutectic morphology is similar to the extracted Cu_6Sn_5 in Figure 1(D). Therefore, it can be concluded that there is no primary Cu_6Sn_5 and only eutectic Cu_6Sn_5 in the Sn-0.7Cu-0.05Al freestanding solder balls.

Table 1. Averaged value and standard deviation of measured area fraction of primary Cu_6Sn_5 and nucleation undercooling of βSn in BGA balls and joints. Values in brackets are the number of samples measured.

	Freestanding solder balls		Joints on Cu substrates	
	Sn-0.7Cu	Sn-0.7Cu-0.05Al	Sn-0.7Cu/Cu	Sn-0.7Cu-0.05Al/Cu
Area fraction of Primary Cu_6Sn_5 [%]	0.24±0.11 (15)	N/A	0.43±0.24 (9)	0.48±0.12 (6)
Nucleation undercooling of βSn [K]	46.3±5.1 (30)	3.6±0.9 (20)	16.5±0.6 (30)	4.5±0.9 (17)

Table 1 summaries the measured area fraction of primary Cu_6Sn_5 in BGA balls. Note that there is zero % primary Cu_6Sn_5 in Sn-0.7Cu-0.05Al balls. The presence of primary Cu_6Sn_5 in hypoeutectic Sn-0.7Cu balls is due to a large nucleation undercooling of βSn, which was measured to be 46.3 ± 5.1 K based on 30 experiments. The mass fraction of primary Cu_6Sn_5 (W_{Cu6Sn5}) in Sn-0.7Cu balls would increase as the βSn nucleation temperature ($T_{nuc}^{\beta Sn}$) decreases according to Equation 1:

$$W_{Cu6Sn5} = \frac{C_0 - f\left(T_{nuc}^{\beta Sn}\right)}{C_{Cu6Sn5} - f\left(T_{nuc}^{\beta Sn}\right)} \times 100\% \qquad \text{Equation 1}$$

Where $C_0 = 0.7\ mass\%$ Cu is the bulk alloy composition, $C_{Cu6Sn5} = 38.7\ mass\%$ Cu is the composition of Cu_6Sn_5, and $f\left(T_{nuc}^{\beta Sn}\right) = 6.5 \times 10^{-9} \times \left(T_{nuc}^{\beta Sn}\right)^{3.456}$ is the fitted extended liquidus line of Cu_6Sn_5 from the Sn-Cu phase diagram in [11]. Using Equation 1, there is a driving force to nucleate primary Cu_6Sn_5 in Sn-0.7Cu once the undercooling reaches 16.9 K and, for the measured nucleation undercooling of 46.3 ± 5.1 K, the mass fraction of Cu_6Sn_5 is predicted to be 0.74 mass% (0.64 vol% Cu_6Sn_5). The somewhat lower measured area fraction in Table 1 might be due to a required nucleation undercooling for Cu_6Sn_5, a required growth undercooling for faceted Cu_6Sn_5 crystal growth and stereology issues related to measuring area fraction in cross-sections through a small number of long rods within a sphere.

The lack of primary Cu_6Sn_5 in Sn-0.7Cu-0.05Al freestanding balls (Figures 1(B) and 2) is due to (i) the reaction of Al with Cu to form Cu_xAl_y intermetallic, reducing the Cu content of the remaining liquid and (ii) the influence of Al on the nucleation undercooling for βSn. For example, samples held isothermally at 250°C for one week contained a layer of particles segregated on the top region due to buoyancy as shown in

Figure 3 (A). SEM-EDX measurements of 15 of the largest black particles (e.g. Figure 3 (B)) gave a mean composition of Al-61at%Cu with a standard deviation of 2 at% and no Sn peaks were present in the EDX spectra. Referring to the most recent Al-Cu phase diagram by Ponweiser et. al. [12], this composition is near the centre of the δ-$Cu_{33}Al_{17}$ phase field.

In addition to causing δ-$Cu_{33}Al_{17}$ to form, Al additions reduced the nucleation undercooling from 46.3 to 3.6 K (see Table 1), similar to past work [1-3]. With an undercooling of only ~4K, only a very slightly hypoeutectic alloy would form primary Cu_6Sn_5 and it is not surprising that primary Cu_6Sn_5 does not form in Sn-0.7Cu-0.05Al freestanding balls. This interpretation is consistent with calculations made using Thermo-Calc software [11], which predicts that δ-$Cu_{33}Al_{17}$ is a primary phase in Sn-0.7Cu-0.05Al and that Cu_6Sn_5 only forms before βSn if the nucleation undercooling for βSn is 44K or higher.

3.2. Sn-0.7Cu freestanding balls and Sn-0.7Cu/Cu BGA joints

Examining Table 1, it can be seen that the area fraction of primary Cu_6Sn_5 is higher in Sn-0.7Cu/Cu joints than in Sn-0.7Cu freestanding balls due to substrate dissolution. Also, it can be seen in Table 1 that the nucleation undercooling for βSn is significantly less in Sn-0.7Cu/Cu joints than in freestanding Sn-0.7Cu balls, which is similar to past studies [13, 14]. The combined influence of Cu dissolution and nucleation undercooling of βSn on the amount of primary Cu_6Sn_5 that forms in Sn-0.7Cu and Sn-0.7Cu/Cu can be understood from the Sn-rich end of the Sn-Cu phase diagram as shown in Figure 4 using data from reference [11]. Note from Equation 1 that the fraction of primary Cu_6Sn_5 depends on the difference between the bulk alloy composition, C_0, and the extended Cu_6Sn_5 liquidus line, which implicitly depends on the nucleation

undercooling of βSn. Figure 4 is a plot of the data for the βSn nucleation temperature in Sn-0.7Cu freestanding balls and in Sn-0.7Cu/Cu joints superimposed on the Sn-Cu phase diagram. The liquid composition for Sn-0.7Cu/Cu joints is plotted as C_{Liq} at 250°C = ~1.25 wt%Cu which is the maximum composition of the liquid above the Cu_6Sn_5 reaction layer (i.e. assuming complete mixing in the liquid). Although the nucleation undercooling of βSn is smaller in Sn-0.7Cu/Cu joints than in Sn-0.7Cu freestanding solder balls (Figure 4) which would result in less primary Cu_6Sn_5 if the two samples had the same Cu content, the increased Cu content in the joints due to substrate dissolution is a more dominant factor and leads to an increase in primary Cu_6Sn_5 fraction as shown in Table 1. Primary Cu_6Sn_5 formation in joints is further complicated by the fact that a portion of the Cu_6Sn_5 that forms on cooling from the peak temperature grows onto the Cu_6Sn_5 reaction layer and the remainder nucleates and grows in the bulk liquid as primary Cu_6Sn_5 rods.

3.3. Sn-0.7Cu/Cu and Sn-0.7Cu-0.05Al/Cu BGA joints

Figure 5 shows that both Sn-0.7Cu/Cu and Sn-0.7Cu-0.05Al/Cu BGA joints contain primary Cu_6Sn_5 crystals in the bulk solder. Figure 5 (A-B) shows typical BSE micrographs of the two BGA joint systems, where the darker particles are primary Cu_6Sn_5 and the brighter background are tin dendrite and eutectic regions. In Figure 5 (A-B) it can be seen that there are more Cu_6Sn_5 crystals in the Al-containing cross-section. Measurements on 5 joints for each composition gave the number of primary Cu_6Sn_5 crystals per mm^2 in Sn-0.7Cu-0.05Al/Cu to be ~7 times more than in Sn-0.7Cu/Cu. Figure 5 (C-D) show the top view of partially etched solder joints, revealing Cu_6Sn_5 crystals protruding from undissolved Sn. In both the cross-sections of Figure 5(A-B) and the etched three dimensional (3D) images of Figure 5(C-D), it can be seen that there are significantly more Cu_6Sn_5 rods in the Al containing sample where they

are also thinner. However, whether the Al addition has caused any significant change in Cu_6Sn_5 length is not clear from two dimensional (2D) sections such as Figure 5(A-B) or partially etched images such as Figure 5(C-D). In particular, note that any small Cu_6Sn_5 rods are likely to have been washed away as the tin dissolved in Figure 5(C-D) and this partial etching technique will be biased towards revealing longer Cu_6Sn_5 rods that still are partially-embedded in the tin.

Therefore, to compare the true 3D length of the primary Cu_6Sn_5 in Sn-0.7Cu/Cu versus Sn-0.7Cu-0.05Al/Cu joints, the length of numerous individual extracted Cu_6Sn_5 crystals, e.g. crystals shown in Figure 5(E-F), were measured. 212 Cu_6Sn_5 rods were measured in Al containing joints and 28 Cu_6Sn_5 rods in Sn-0.7Cu/Cu joints in 8 samples of each composition. The data are summarised as a histogram of primary Cu_6Sn_5 rod length in Figure 6. The number of primary Cu_6Sn_5 rods in Figure 6 cannot be used to quantify the number of Cu_6Sn_5 crystals per unit volume because some rods were lost during the etching and washing process. However, the fact that the mean length of Cu_6Sn_5 rods decreased by a factor of ~4 after Al additions is apparent, as are the significantly more numerous Cu_6Sn_5 rods in Sn-0.7Cu-0.05Al/Cu joints. Care was taken to check whether rods had fractured during dissolution and extraction: most ends of the measured rods had the morphology expected of a faceted growth tip rather than a fracture surface. The only exception was that some rods in Sn-0.7Cu/Cu samples were fractured, indicating that the mean Cu_6Sn_5 rod length in Sn-0.7Cu/Cu is actually even higher than that shown in Figure 6. Note also from Figure 6 that, in Sn-0.7Cu/Cu joints and Sn-0.7Cu balls, some Cu_6Sn_5 rods grow to nearly 90% of the solder ball diameter, which was not apparent in 2D sections such as Figure 5(A-B).

A challenge in studying grain refinement of primary intermetallics in solder joints is that additions often affect the volume fraction of intermetallic that forms in addition to their influence on the number of nucleation events. However, in the case of Sn-0.7Cu/Cu and Sn-0.7Cu-0.05Al/Cu joints, the fraction of primary Cu_6Sn_5 is similar with and without the Al additions (Table 1) and it can be concluded that the decreased Cu_6Sn_5 size and increased number of Cu_6Sn_5 crystals (Figure 6) is due to an increased number of Cu_6Sn_5 nucleation events per unit volume with the Al addition.

Figure 5(E) shows a SE-SEM micrograph of typical extracted primary Cu_6Sn_5 crystals in Sn-0.7Cu/Cu joints, showing the long (100s of μm) hexagonal rod morphology. The Cu_6Sn_5 rods in Sn-0.7Cu/Cu joints have similar morphologies to those in the freestanding solder balls as shown in Figure 1 (C). Figure 5(F) shows two types of typical morphologies of primary Cu_6Sn_5 in Sn-0.7Cu-0.05Al/Cu joints. The top two crystals in Figure 5(F) has the morphology of a hexagonal rod similar to those in Sn-0.7Cu BGA balls and joints, while the bottom crystal in Figure 5(F) has an 'X-shape'. Note that the angle between arms of the X-shape here is quite constant, which is different to the reported X-shape of Cu_6Sn_5 in binary Sn-Cu system [15], where the angles between arms are more random. Note that Figure 5 (E-F) are at the same magnification.

In Table 1, it can be seen that the area fraction of primary Cu_6Sn_5 is similar in joints with and without Al. This shows that substrate dissolution compensates for the Cu that reacts with Al to form δ-$Cu_{33}Al_{17}$. Note also that the nucleation undercooling for βSn is similar in Sn-0.7Cu-0.05Al freestanding balls and Sn-0.7Cu-0.05Al/Cu joints, and that the undercooling is less in Sn-0.7Cu-0.05Al/Cu joints than in Sn-0.7Cu/Cu joints.

A quantitative understanding of the combined influence of Cu dissolution and nucleation undercooling of βSn on primary Cu_6Sn_5 formation in Sn-0.7Cu-0.05Al/Cu joints can be obtained from Figure 7, which is based on Thermo-Calc calculations assuming the Sn-Cu-Al phase equilibria in the TCSLD v.3 database [11].

Figure 7 (A) is the Sn-Cu-Al isothermal section at 250°C based on ref [11]. With the TCSLD3 database, Thermo-Calc predicts that β Cu-Al phase (BCC_B2) should be an equilibrium phase at 250°C but, since it was not observed in Sn-0.7Cu-0.05Al/Cu joints, this phase was omitted from the calculations. In Figure 7(A), the "□" symbol denotes the composition Sn-0.7Cu-0.05Al which is in the L+δ$Cu_{33}Al_{17}$ two-phase region at 250°C. The relevant L+δ$Cu_{33}Al_{17}$ tie line is plotted as a dashed line and the equilibrium liquid composition of freestanding balls at 250°C is marked with a "○" symbol. During reactive dissolution of the Cu substrate, the liquid will become enriched in Cu, following the 250°C contour of the liquidus surface until it reaches the corner of the L+Cu_xAl_y+Cu_6Sn_5 tie-triangle when the liquid is in equilibrium with both the Cu_xAl_y particles and the Cu_6Sn_5 reaction layer. This liquid composition is marked with a "△" symbol. Note that Thermo-Calc also predicts that there is a transformation from δ$Cu_{33}Al_{17}$ to γ_1-Cu_9Al_4 as the liquid becomes enriched in Cu. However, these phases are crystallographically very similar (as discussed in ref [7]) and it is not important for this paper whether or not δ transforms into γ_1-Cu_9Al_4. Figure 7(B) is a plot of the development of primary Cu_6Sn_5 during cooling from the peak reflow temperature of 250°C for Sn-0.7Cu-0.05Al/Cu joints (assuming a liquid composition marked with a "△" symbol from Figure 7(A)) as well as for Sn-0.7Cu/Cu joints and Sn-0.7Cu and Sn-0.7Cu-0.05Al freestanding balls. The βSn phase has been omitted to calculate the development of primary Cu_6Sn_5 as the liquid supercools with respect to βSn. 'X'

symbols denote the mean measured nucleation undercooling for βSn in each solder/substrate combination. The Thermo-Calc predictions in Figure 7(B) are in reasonable agreement with our results. For example, primary Cu_6Sn_5 is predicted to form in Sn-0.7Cu but not Sn-0.7Cu-0.05Al freestanding balls, and the fraction of primary Cu_6Sn_5 in Sn-0.7Cu/Cu and Sn-0.7Cu-0.05Al/Cu joints are similar for the levels of undercooling measured.

3.4. Heterogeneous nucleation mechanism of Cu_6Sn_5

Microstructural analysis suggested that the smaller and more numerous primary Cu_6Sn_5 crystals in Sn-0.7Cu-0.05Al/Cu joints (Figure 6) are due to heterogeneous nucleation of Cu_6Sn_5 on δ-$Cu_{33}Al_{17}$ particles. Figure 8 shows a series of BSE micrographs of primary Cu_6Sn_5 particles in Sn-0.7Cu-0.05Al/Cu containing or sharing an interface with some black particles. These particles have similar morphology to those in the holding sample in Figure 3 and are very likely to be the same δ-$Cu_{33}Al_{17}$ phase. They are, however, too small for accurate SEM-EDX and it is possible that δ-$Cu_{33}Al_{17}$ has transformed into γ$_1$-Cu_9Al_4 as predicted by Figure 7(A). As we have shown previously, the crystallographic similarities between δ-$Cu_{33}Al_{17}$ and γ$_1$-Cu_9Al_4 mean that both phases form a similar lattice match to Cu_6Sn_5 and we will refer to the phase as δ-$Cu_{33}Al_{17}$ for the remainder of this paper.

Examination of cross-sections of Cu_6Sn_5 crystals containing δ-$Cu_{33}Al_{17}$ showed that there were often reproducible facet relationships between the Cu_6Sn_5 and δ-$Cu_{33}Al_{17}$ particles. A typical example can be found in Figure 8(E), where the shorter edge (marked by red dashed line) of the rectangular δ-$Cu_{33}Al_{17}$ is parallel to a Cu_6Sn_5 facet, and the longer edge (blue dashed line) is parallel to the second nearest corners of the

Cu_6Sn_5 crystal. It is possible to infer the Cu_6Sn_5 habit planes at δ-$Cu_{33}Al_{17}$ - Cu_6Sn_5 interfaces from this commonly-found geometrical observation because hexagonal rods of Cu_6Sn_5 grow with reproducible growth facets. Figure 9 shows the indexing of the facets of a primary Cu_6Sn_5 rod. According to the EBSD pattern in Figure 9(B) and measured unit cell orientation in Figure 9(A), it can be seen that the facets of the hexagonal Cu_6Sn_5 rods are the $\{1\bar{1}00\}$-type prism planes. In Figure 9(C), the hexagonal facets of an extracted Cu_6Sn_5 rod are labelled as $\{1\bar{1}00\}$, and the growth direction can be seen to be [0001].

Therefore, the habit plane marked by the short red dashed line in Figure 8(E) is parallel to a $\{1\bar{1}00\}$ of Cu_6Sn_5 and the habit plane marked by the blue dashed line is parallel to a $\{11\bar{2}0\}$ of Cu_6Sn_5. These two families of planes in Cu_6Sn_5 are exactly those found to nucleate on δ-$Cu_{33}Al_{17}$ and γ_1-Cu_9Al_4 in Sn-4Cu-0.2Al in our previous detailed crystallographic study [7]. Therefore, similar to Sn-4Cu-0.2Al, it can be concluded that a nucleation orientation relationship between δ-$Cu_{33}Al_{17}$ and Cu_6Sn_5, OR1, is:

$\{1\bar{1}00\}_{Cu33Al17}\|\{1\bar{1}00\}_{Cu6Sn5}$ with $[0001]_{Cu33Al17}\|[0001]_{Cu6Sn5}$

with $\{1\bar{1}00\}$ and $\{11\bar{2}0\}$ as the two interfacial planes (habit planes), using the hexagonal setting for rhombohedral δ-$Cu_{33}Al_{17}$.

If the rhombohedral setting is used instead for δ-$Cu_{33}Al_{17}$, the same OR1 is:

$(10\bar{1})_{Cu33Al17}\|(1\bar{2}10)_{Cu6Sn5}$ with $[111]_{Cu33Al17} \| [0001]_{Cu6Sn5}$

with $(10\bar{1})_{Cu33Al17}\|(1\bar{2}10)_{Cu6Sn5}$ or $(2\bar{1}\bar{1})_{Cu33Al17}\|(1\bar{1}00)_{Cu6Sn5}$.

A second orientation relationship, OR2, is also consistent with the facet relationship, as follows:

$(1\bar{2}10)_{Cu33Al17}\|(1\bar{2}10)_{Cu6Sn5}$ with $[\bar{2}021]_{Cu33Al17}\|[0001]_{Cu6Sn5}$

with interfacial plane as $(1\bar{2}10)_{Cu33Al17}||(1\bar{2}10)_{Cu6Sn5}$ in the hexagonal form;

or $(10\bar{1})_{Cu33Al17}||(1\bar{2}10)_{Cu6Sn5}$ and $[1\bar{1}1]_{Cu33Al17}||[0001]_{Cu6Sn5}$

with interfacial plane $(10\bar{1})_{Cu33Al17}||(1\bar{2}10)_{Cu6Sn5}$ in the rhombohedral form.

Note that the ORs are presented using hexagonal η-Cu_6Sn_5 [16, 17] because this phase is expected to have been present during primary Cu_6Sn_5 prior to superstructure ordering to monoclinic η'-Cu_6Sn_5 at lower temperature [18, 19].

The two ORs offer an interesting insight into the 'X-shape' of primary Cu_6Sn_5 crystals in Figure 5(F), which are commonly seen in Sn-0.7Cu-0.05Al/Cu joints and not in Sn-0.7Cu/Cu joints. The acute angle between arms of the 'X-shaped' Cu_6Sn_5 is 70°±2° from more than 10 measured crystals similar to that in Figure 5(F). Assuming that the four arms of the X-shape all nucleate on one single δ-$Cu_{33}Al_{17}$ particle and the growth direction of the four arms are all $[0001]_{Cu6Sn5}$, then one of the Cu_6Sn_5 arms is parallel with $[111]_{Cu33Al17}$, i.e. OR1, and the other nearest arm would be parallel with $[1\bar{1}1]_{Cu33Al17}$, i.e. OR2. Because the rhombohedral δ-$Cu_{33}Al_{17}$ has a very nearly cubic unit cell, the angle between $[111]_{Cu33Al17}$ and $[1\bar{1}1]_{Cu33Al17}$ in the rhombohedral unit cell is ~70.5°, which is consistent with the measured angle between the 'X-shaped' Cu_6Sn_5 arms. Therefore, the formation of the 'X-shaped' Cu_6Sn_5 is likely to be due to multiple nucleation events on a single δ-$Cu_{33}Al_{17}$ particle with two different nucleation ORs. Further work is required to prove this idea.

The interfacial planes between δ-$Cu_{33}Al_{17}$ and Cu_6Sn_5 in these ORs give a good planar lattice match with only ~2.5% mismatch as shown in ref [7]. This is consistent with δ-$Cu_{33}Al_{17}$ being a potent nucleant for Cu_6Sn_5 with low interfacial energy and suggests

that the epitaxial nucleation of Cu_6Sn_5 on δ-$Cu_{33}Al_{17}$ is the main cause of the Cu_6Sn_5 grain refinement. The presence of δ-$Cu_{33}Al_{17}$ in samples held for one week at 250°C (Figure 3) also shows that δ-$Cu_{33}Al_{17}$ particles do not fully-melt during reflow with a peak temperature of 250°C and, therefore, δ-$Cu_{33}Al_{17}$ are present in the liquid prior to primary Cu_6Sn_5 nucleation. The average size of δ-$Cu_{33}Al_{17}$ in Sn-0.7Cu-0.05Al/Cu joints is ~1μm (Figure 8) and the average size of floating δ-$Cu_{33}Al_{17}$ particles after one week at 250°C is only slightly larger at ~1-2 μm (Figure 3). This shows that the δ-$Cu_{33}Al_{17}$ particles are stable in the melt and coarsen particularly slowly, even when in a liquid matrix.

While heterogeneous nucleation on δ-$Cu_{33}Al_{17}$ seems to be the main cause of Cu_6Sn_5 grain refinement in Sn-0.7Cu-0.05Al/Cu joints, it is probable that other factors play some role. For example, it is not known how Al alters the Cu_6Sn_5-L interfacial energy.

4. Conclusions

The formation of primary (pro-eutectoid) Cu_6Sn_5 rods has been studied in Sn-0.7Cu and Sn-0.7Cu-0.05Al freestanding BGA balls and in Sn-0.7Cu/Cu and Sn-0.7Cu-0.05Al/Cu joints. For a constant reflow profile (time liquid, peak temperature and cooling rate), primary Cu_6Sn_5 formation in the bulk solder is shown to be affected by three main factors:

(i) the increasing Cu content of the liquid due to substrate dissolution

(ii) the change in phase equilibria due to the Al and Cu addition. In particular, the reaction of Al with Cu to form δ-$Cu_{33}Al_{17}$ in the liquid prior to Cu_6Sn_5 nucleation.

(iii) the degree of nucleation undercooling for βSn (similar to large Ag_3Sn blades in SAC solders)

It is demonstrated that the size of primary Cu_6Sn_5 rods in BGA balls and joints can be greatly underestimated by analysing 2D sections and that the true 3D length of primary Cu_6Sn_5 rods can span almost the entire 500μm solder ball in Sn-0.7Cu/Cu joints and Sn-0.7Cu balls.

A key result from this work is that a 0.05wt% Al addition to Sn-0.7Cu solder can significantly reduce the size of primary Cu_6Sn_5 crystals during soldering to Cu substrates. The reduced size of primary Cu_6Sn_5 is accompanied by an increase in the number of Cu_6Sn_5 particles per unit volume and the total fraction of Cu_6Sn_5 is similar in Sn-0.7Cu/Cu and Sn-0.7Cu-0.05Al/Cu joints. The grain refinement mechanism is heterogeneous epitaxial nucleation of Cu_6Sn_5 on δ-$Cu_{33}Al_{17}$ particles. These phases are found to form interfaces with a lattice mismatch of ~2.5% and it is likely that the nucleation interface is coherent and of low interfacial energy. The δ-$Cu_{33}Al_{17}$ particles

are found to be stable in the melt at 250°C and, therefore, do not melt during reflow. The size of active δ-$Cu_{33}Al_{17}$ nuclei was <1μm in Sn-0.7Cu-0.05Al/Cu joints and δ-$Cu_{33}Al_{17}$ are shown to coarsen very slowly in the melt.

These findings indicate that Al additions might be useful at decreasing the size of primary Cu_6Sn_5 crystals in BGA/Cu joints.

5. Acknowledgments

We are grateful for support from Nihon Superior Co., Ltd. and UK EPSRC grant EP/M002241/1.

6. References

[1] I.E. Anderson, J.W. Walleser, J.L. Harringa, F. Laabs, A. Kracher, *J. Electron. Mater.* 38, 2770 (2009)
[2] A. Kantarcıoğlu, Y.E. Kalay, *Mater. Sci. Eng. A* 593, 79 (2014)
[3] H.R. Kotadia, O. Mokhtari, M. Bottrill, M.P. Clode, M.A. Green, S.H. Mannan, *J. Electron. Mater.* 39, 2720 (2010)
[4] A.J. Boesenberg, I.E. Anderson, J.L. Harringa, *J. Electron. Mater.* 41, 1868 (2012)
[5] K.N. Reeve, I.E. Anderson, C.A. Handwerker, *J. Electron. Mater.* 44, 842 (2015)
[6] H.R. Kotadia, A. Panneerselvam, O. Mokhtari, M.A. Green, S.H. Mannan, *J. Appl. Phys.* 111, (2012)
[7] J.W. Xian, S.A. Belyakov, T.B. Britton, C.M. Gourlay, *J. Alloys Comp.* 619, 345 (2015)
[8] S. McDonald, K. Nogita, J. Read, T. Ventura, T. Nishimura, *J. Electron. Mater.* 42, 256 (2013)
[9] E.H. Kisi, J.D. Browne, *Acta Crystallogr. Sect. B* 47, 835 (1991)
[10] L. Arnberg, S. Westman, *Acta Crystallogr. Sect. A* 34, 399 (1978)
[11] Thermo-Calc, TCSLD Database version 3.0, (2015)
[12] N. Ponweiser, C.L. Lengauer, K.W. Richter, *Intermetallics* 19, 1737 (2011)
[13] M.G. Cho, S.K. Seo, H.M. Lee, *Mater. Trans.* 50, 2291 (2009)
[14] Y.-c. Huang, S.-w. Chen, K.-s. Wu, *J. Electron. Mater.* 39, 109 (2010)
[15] P. Zhou, H.J. Kang, F. Cao, Y.A. Fu, T.Q. Xiao, T.M. Wang, *J. Mater. Sci.: Mater. Electron.* 25, 4538 (2014)
[16] B. Peplinski, G. Schulz, D. Schultze, E. Schierhorn, *Mater. Sci. Forum* 228, 577 (1996)
[17] K. Nogita, C.M. Gourlay, T. Nishimura, *JOM* 61, 45 (2009)
[18] K. Nogita, C.M. Gourlay, S.D. McDonald, Y.Q. Wu, J. Read, Q.F. Gu, *Scripta Mater.* 65, 922 (2011)
[19] A.K. Larsson, L. Stenberg, S. Lidin, *Acta Crystallogr. Sect. B* 50, 636 (1994)

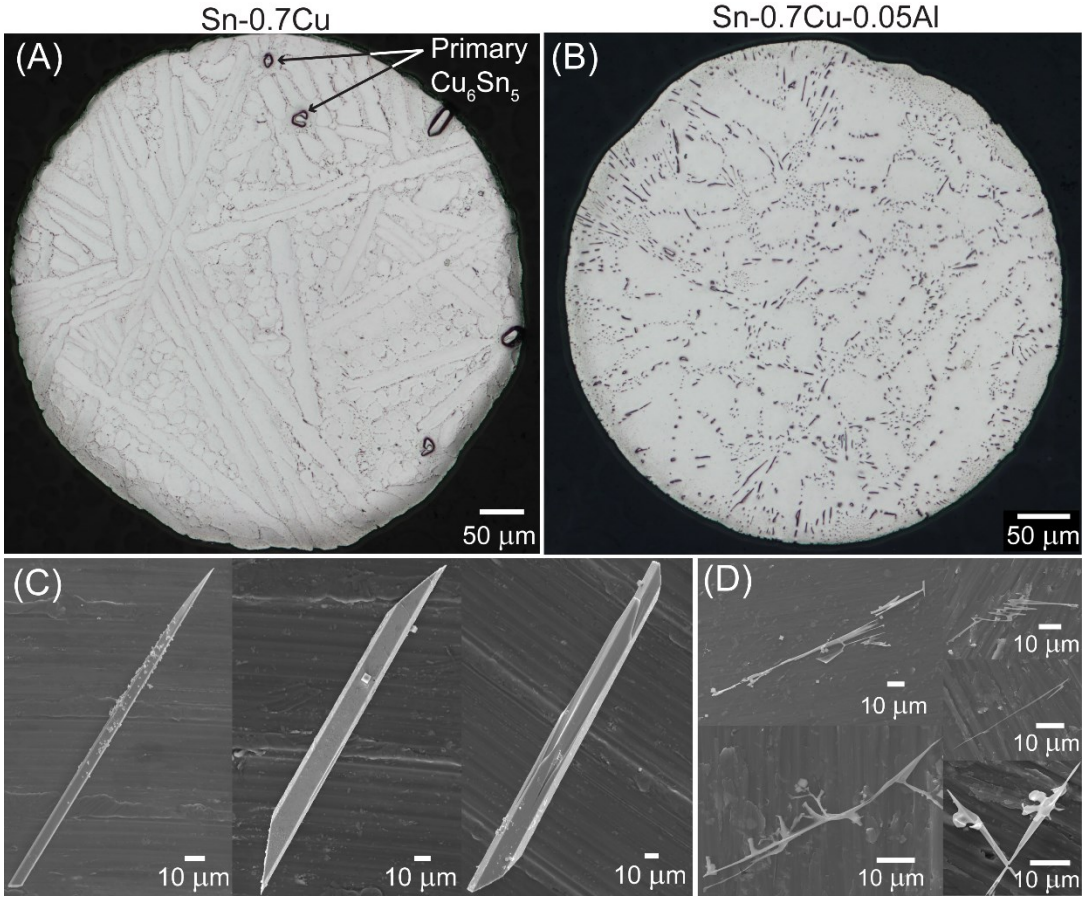

Figure 1. (A)-(B): Typical microstructures of freestanding ~500μm solder balls cooled at 0.33K/s in a DSC. (A) Sn-0.7Cu, (B) Sn-0.7Cu-0.05Al. (C)-(D) Typical extracted Cu_6Sn_5 crystals from freestanding solder balls. (C) Sn-0.7Cu and (D) Sn-0.7Cu-0.05Al. N.B. crystals in (D) are eutectic Cu_6Sn_5.

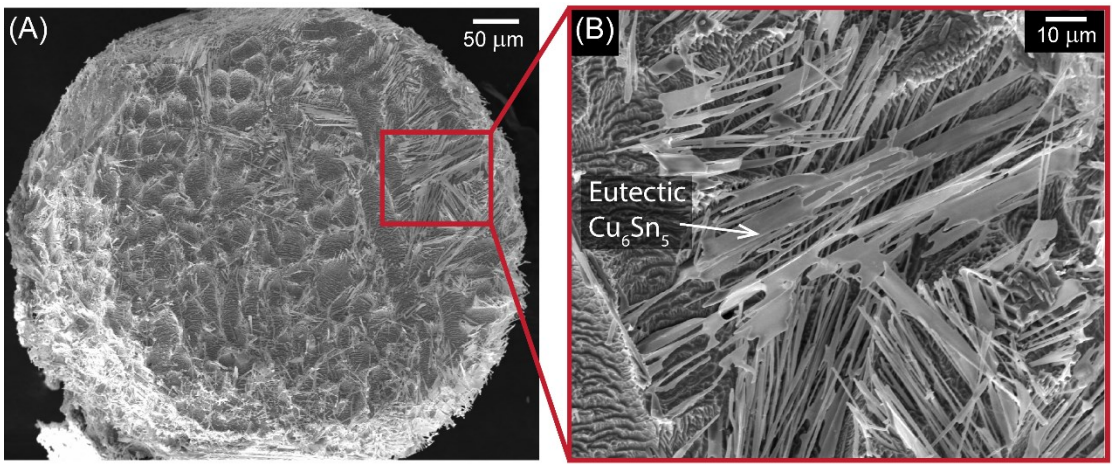

Figure 2. Typical BSE images of Sn-0.7Cu-0.05Al BGA balls after shallow etching. (A) A whole solder ball and (B) a high magnification micrograph of eutectic Cu_6Sn_5 of similar lengthscale to Fig. 1(D).

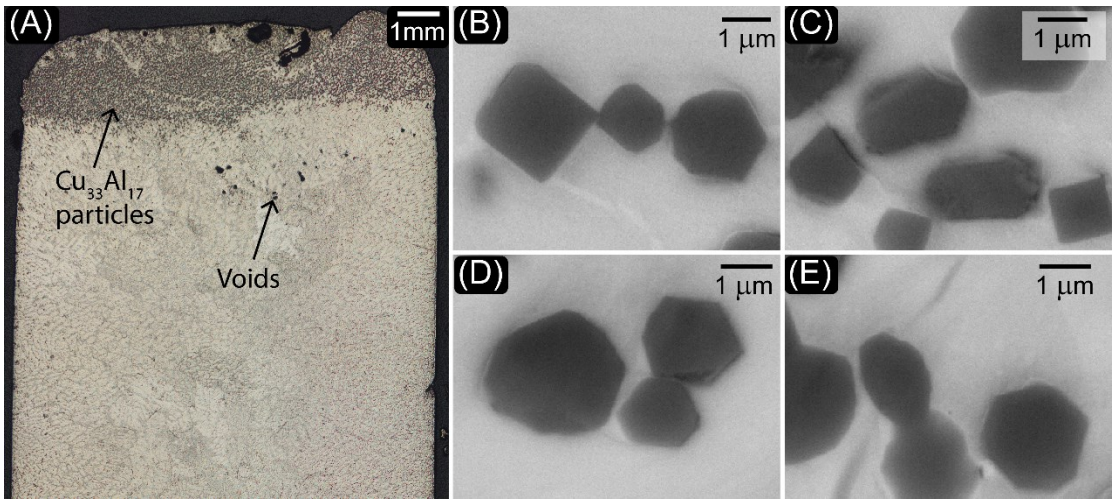

Figure 3. (A) Optical image of the top region of a Sn-0.7Cu-0.05Al alloy held at 250°C for one week. (B)-(E) Typical higher magnification BSE micrographs of the δ-$Cu_{33}Al_{17}$ particles segregated at the top due to buoyancy.

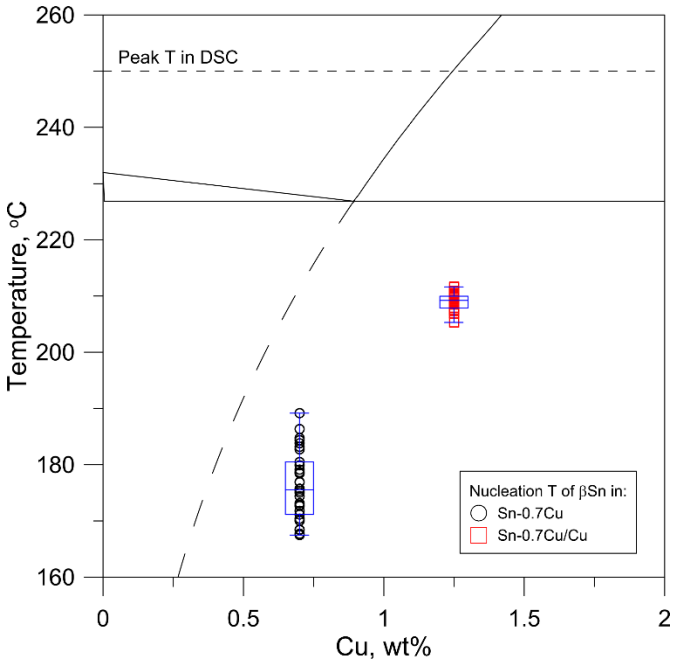

Figure 4. Partial Sn-Cu phase diagram with best-fit extended Cu_6Sn_5 liquidus line based on data from [11]. Measured nucleation temperatures of βSn in ~500µm BGA balls and joints are marked, and boxplots summarise the statistics from >30 experiments. The Sn-0.7Cu/Cu joint data is plotted assuming a liquid composition that is saturated in Cu at the DSC peak temperature.

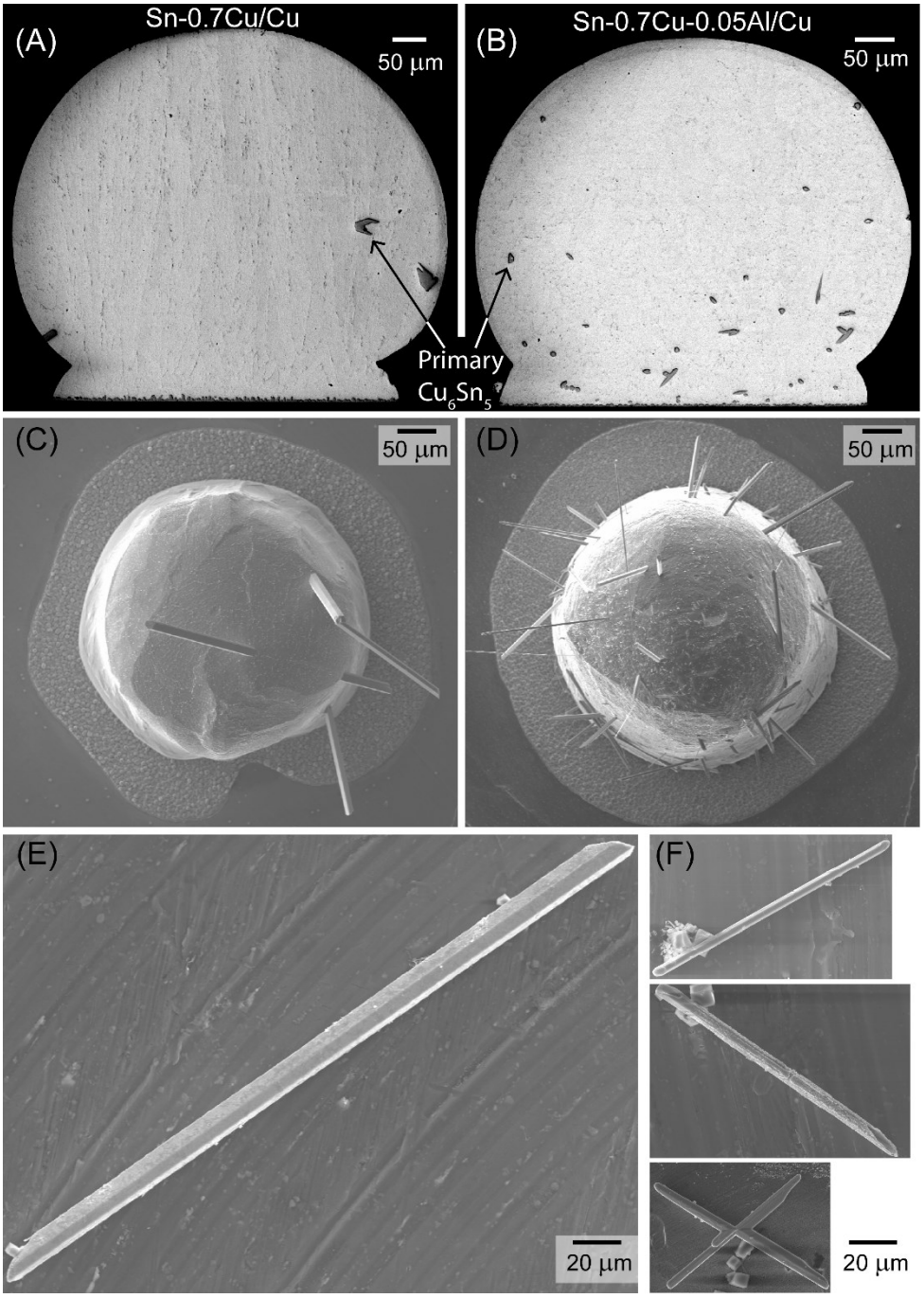

Figure 5. (A-B) Typical microstructures of ~500μm BGA/Cu joints cooled at 0.33K/s in a DSC. (C-D) Top view of partially etched solder joints. (E-F) Typical extracted primary Cu_6Sn_5 crystals. (A,C,E) Sn-0.7Cu/Cu, (B,D,F) Sn-0.7Cu-0.05Al/Cu.

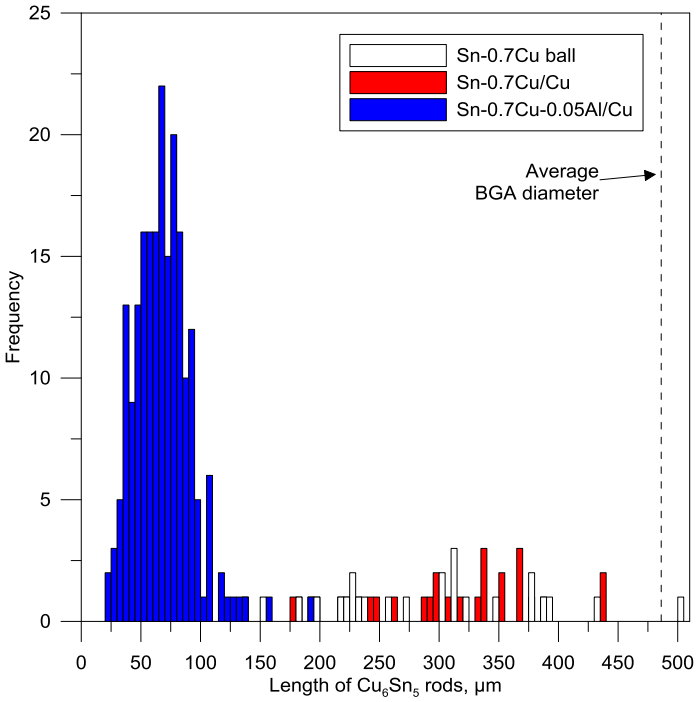

Figure 6. A histogram of the length of primary Cu_6Sn_5 rods in BGA freestanding balls and BGA/Cu joints cooled at 0.33K/s from 250°C in a DSC. Note that freestanding Sn-0.7Cu-0.05Al balls contained no primary Cu_6Sn_5.

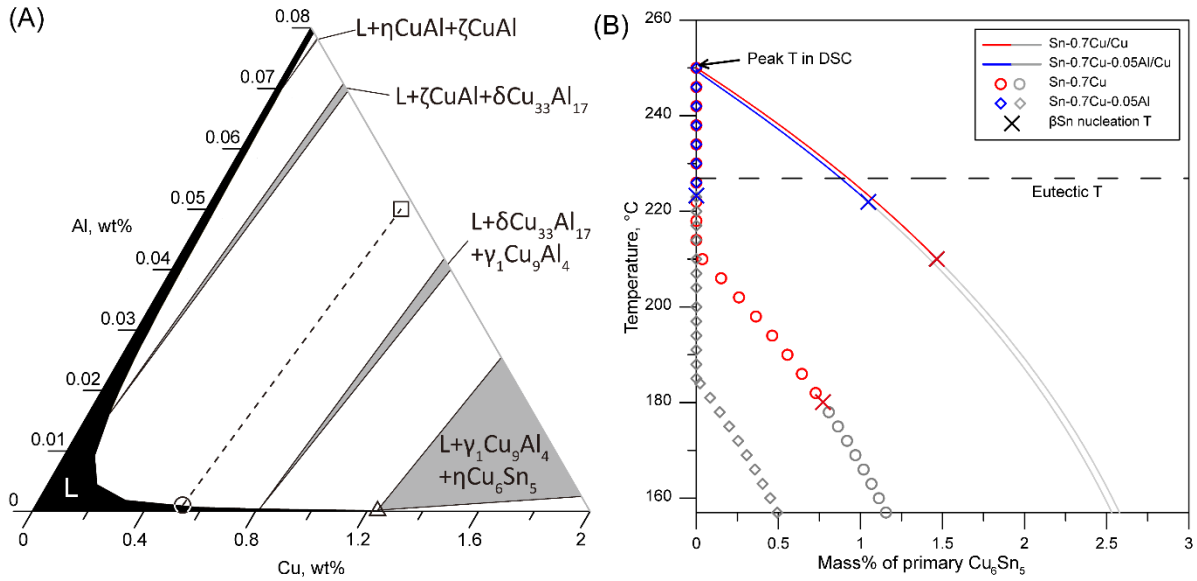

Figure 7. (A) Sn-Cu-Al isothermal section at 250°C based on [11]. (B) Solidification path of primary Cu_6Sn_5 during cooling from 250°C in Sn-0.7Cu-0.05Al, Sn-0.7Cu BGA balls and Sn-0.7Cu-0.05Al/Cu, Sn-0.7Cu/Cu joints.

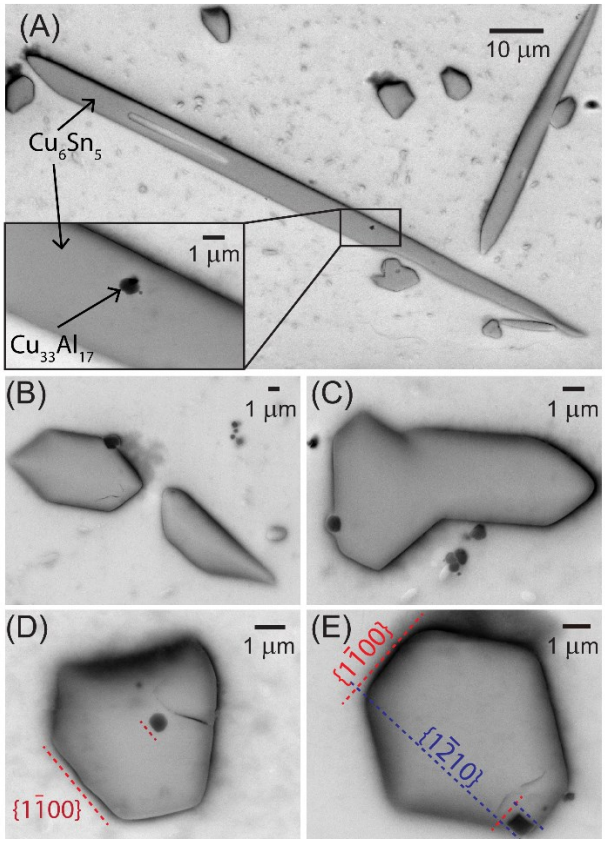

Figure 8. Typical BSE micrographs of Cu_6Sn_5 particles containing Cu-Al particles in Sn-0.7Cu-0.05Al/Cu joints. Facet relationships between δ-$Cu_{33}Al_{17}$ particles and Cu_6Sn_5 are drawn in (D) and (E).

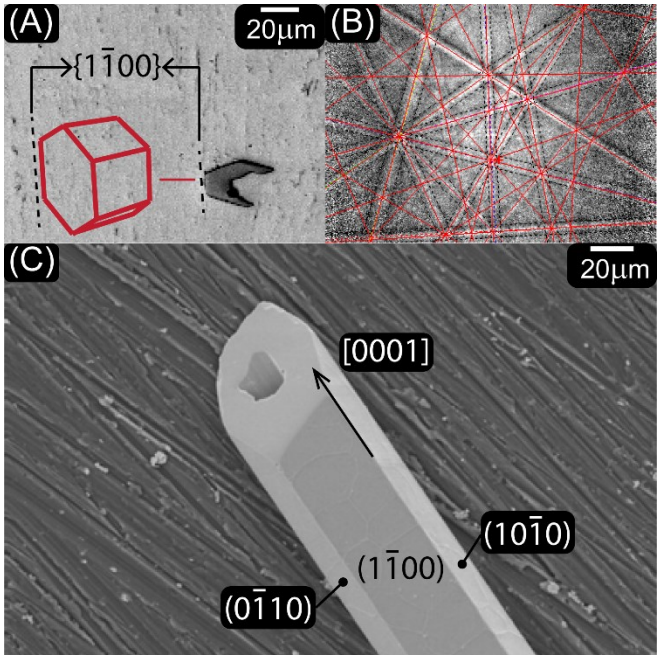

Figure 9. (A) BSE micrograph of the cross section of a primary Cu_6Sn_5 in a Sn-0.7Cu/Cu BGA joint. (B) EBSD pattern of the Cu_6Sn_5 in (A) which is indexed as hexagonal η-Cu_6Sn_5 [16,17]. Note that the measured orientation of the unit cell is outlined in (A) showing the facets in the micrograph are $\{1\bar{1}00\}$-type. (C) An extracted hollow Cu_6Sn_5 hexagonal-rod in Sn-0.7Cu with labelled facets.